Observation of Transient Anions which Do Not Decay through Dissociative Electron Attachment: New Pathways for Radiosensitization

Ana I Lozano, Fábris Kossoski, Francisco Blanco, Paulo Limão-Vieira, Márcio Varella, Gustavo García

▶ **To cite this version:**

Ana I Lozano, Fábris Kossoski, Francisco Blanco, Paulo Limão-Vieira, Márcio Varella, et al.. Observation of Transient Anions which Do Not Decay through Dissociative Electron Attachment: New Pathways for Radiosensitization. Journal of Physical Chemistry Letters, 2022, 13 (30), pp.7001-7008. 10.1021/acs.jpclett.2c01704 . hal-03818091

HAL Id: hal-03818091
https://hal.science/hal-03818091

Submitted on 17 Oct 2022

HAL is a multi-disciplinary open access archive for the deposit and dissemination of scientific research documents, whether they are published or not. The documents may come from teaching and research institutions in France or abroad, or from public or private research centers.

L'archive ouverte pluridisciplinaire **HAL**, est destinée au dépôt et à la diffusion de documents scientifiques de niveau recherche, publiés ou non, émanant des établissements d'enseignement et de recherche français ou étrangers, des laboratoires publics ou privés.

Observation of Transient Anions which Do Not Decay through Dissociative Electron Attachment: New Pathways for Radiosensitization

Ana I. Lozano[1,2,*], Fábris Kossoski[3,*], Francisco Blanco[4], Paulo Limão-Vieira[2], Márcio T. do N. Varella[5], and Gustavo García[1,6]

[1]*Instituto de Física Fundamental, Consejo Superior de Investigaciones Científicas, Serrano 113-bis, 28006 Madrid, Spain.*

[2]*Laboratório de Colisões Atómicas e Moleculares, CEFITEC, Departamento de Física, Faculdade de Ciências e Tecnologia, Universidade NOVA de Lisboa, 2829-516 Caparica, Portugal.*

[3]*Laboratoire de Chimie et Physique Quantiques (UMR 5626), Université de Toulouse, CNRS, UPS, 31062 Toulouse, France.*

[4]*Departamento de Física Atómica, Molecular y Nuclear, Universidad Complutense de Madrid, 28040 Madrid, Spain.*

[5]*Instituto de Física, Universidade de São Paulo, Rua do Matão 1731, 05508-090 São Paulo, Brazil.*

[6]*Centre for Medical Radiation Physics, University of Wollongong, NSW, Australia.*

Abstract: Low-energy electrons (LEEs) can very efficiently induce bond breaking via dissociative electron attachment (DEA). While DEA is ubiquitous, the importance of other reactions initiated by LEEs remains much more elusive. Here, we looked into this question by measuring highly accurate total cross sections (TCSs) for electron scattering from 1-methyl-5-nitroimidazole (1M5NI), a model radiosensitizer. The small uncertainty and high energy resolution allow us to identify many resonant features related to the formation of transient anions. Besides providing novel insights about DEA reactions through the lower-lying resonances, our key finding is that the higher-lying resonances do not undergo DEA, implying alternative decay channels with significant cross sections. In particular, dissociation into two neutral fragments is probably involved in the case of 1M5NI. This finding has direct implications to the understanding of LEE-induced chemistry, particularly in the fundamental processes underlying the radiosensitization activity.

TOC Graphic

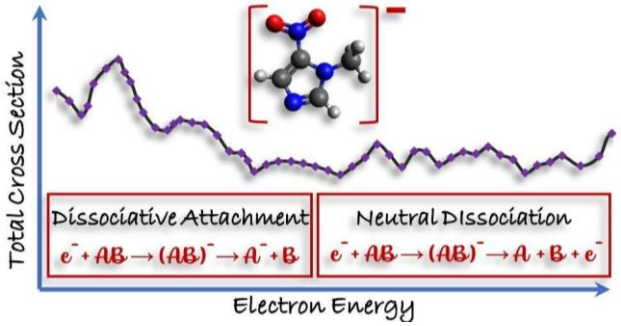

When a free electron encounters a molecule, the energy from the impinging electron can be efficiently transferred to the molecular target via the formation of a transient anion state[1]. Such states are resonances, meaning they can decay by detachment of the extra electron. When they have long lifetimes against autodetachment, dissociative electron attachment (DEA) becomes likely[2]. Most molecules are known to undergo DEA, the roles of such processes being numerous and subject of many studies[2-5]. Much less is known about the nature and relevance of other chemical processes initiated by electrons, e.g., neutral dissociation. Only recently, bond breaking by the action of a catalytic electron has been theoretically proposed[6,7], and experimentally verified[8]. This is also a resonant process, taking place via the formation of a transient anion. In this case, however, the electron is released along the reaction, whereas in DEA it remains attached to one of the fragments. Experimentally, DEA can present sizable cross sections, and the presence of the precursor resonance can be inferred by measurements of the produced ion yields[1]. Alternatively, the resonances can be experimentally probed via accurate measurements of total cross sections (TCSs) for electron scattering[9,10], where they usually manifest as prominent features. A remarkable advantage of electron transmission[11] (TCS measurements in particular) over DEA experiments is that resonances leave a signature in the cross sections regardless of their decaying mechanisms. As such, transmission experiments thus allow us to trace other decay processes besides DEA, although with no possibility of discerning the process itself.

The role of electron-induced chemistry is increasingly recognized within the context of radiosensitization[12-16], although it is a prevalent mechanism in discharges, plasma processing, nanolithography, among many others[17-19]. The efficacy of radiotherapy treatments can be significantly improved when deployed in conjunction with radiosensitizer compounds[20-22]. These molecules act by enhancing the radiosensitivity of tumor tissues/cells, thus allowing to reduce the doses delivered, while minimizing the damage induced by radiotherapy in the neighboring healthy tissues. Although the underlying mechanisms of radiosensitivity still remain poorly understood, the production and subsequent chemistry mediated by free radicals certainly plays a key role[14,15]. In particular, low-energy electrons (<10 eV), generated in large numbers along the track of the primary ionization radiation[23,24], can efficiently produce free radicals via DEA processes[2]. This mechanism has motivated the international scientific community to investigate DEA reactions of biologically relevant molecules, with particular relevance to model radiosensitizers[25]. In contrast, much less is known about the relevance of other electron-induced processes that do not lead to charged fragments.

Nitroimidazoles (NIs) comprise one of the main classes of candidate radiosensitizers under investigation, in view of their high electron affinities[21,26]. The most studied NIs are nimorazole, metronidazole, and misonidazole, the first one being currently employed to treat some types of carcinomas in Denmark[27]. Their radiosensitizing effect is believed to stem from the action of low-energy electrons, which would produce reactive species when interacting with the NIs[28-33]. Specifically, DEA reactions have been implied as the most relevant underlying process for smaller NIs[28-30]. More recently, however, the radiosensitivity of nimorazole[31] and metronidazole[33] has been linked to the formation of the non-decomposed anion via associative electron attachment. Here we put forward a new route for the radiosenisitization of NIs, based on the production of neutral fragments via the action of catalytic electrons. It is also worth mentioning that NIs have been proposed as potential candidates for high-energy materials[35-38] due to their high heat of formation[39]. These aspects have motivated several studies on the decomposition of NIs upon collisions with different projectiles[28-33,37,38,40-

[43]. Of major relevance to the present study, Tanzer *et al.*[28,29] carried out two experimental investigations on DEA to 4(5)-nitroimidazole (4(5)NI) and its methylated derivatives, 1-methyl-5-nitroimidazole (1M5NI) and 1-methyl-4-nitroimidazole (1M4NI), where they obtained the ion yields as a function of the electron impact energy. Several fragment anions were detected between 2 and 6 eV, for the three molecules, despite some differences in their fragmentation pattern. They found that methylation quenches decomposition at the lower impact energies (<2 eV) and, importantly, that no DEA reactions occur above ~6 eV.

In light of the above motivations, here we looked into the electron-molecule interaction by measuring the first set of total cross sections for 1M5NI, covering a wide energy range (1 to 300 eV). The choice for 1M5NI was motivated by (i) its structural similarity to the larger nitroimidazolic radiosensitizers nimorazole and metronidazole, (ii) the availability of DEA data[28,29], and (iii) the feasibility for measuring the TCS (as discussed below). Energies below 1 eV could not be probed due to a limitation of our experimental setup. Moreover, with the help of multireference configuration interaction (MRCI)[44] calculations, we provide several novel insights about the nature of the lower-lying resonances and their correspondence to the DEA decay channels. The most important result concerns the observation of several unexpected resonances in the TCS, which have no parallel to the previous experiments on DEA. The obtained TCS is further used to assess the accuracy of two different *ab-initio* scattering calculations, the Schwinger multichannel (SMC) method[45,46] for the lower impact energies (1 to 15 eV), and the independent atom model with the screening-corrected additivity rule plus interference (IAM-SCAR+I) method[47-50] for the higher energies (15 to 300 eV).

The present TCS measurements are noteworthy on their own. As far as we are aware, few such measurements for gas-phase molecules which are solid at room temperature have ever been performed, just for fructose[51], thymine[52], phenol[53], and *para*-benzoquinone[54] (*p*BQ). For the former two molecules, however, only normalized (not absolute) values have been reported, most probably due to the difficulty of assessing the vapor pressure inside the scattering cell[10,51,52]. Thus, the only sets of absolute TCS for solid molecular samples have been given a few years ago for phenol[53] and *p*BQ[54], with our current experimental setup (though in different configurations[53,54]). Here, we ventured into performing TCS measurements for 1M5NI, a molecule having a vapor pressure at room temperature of ~1.7×10^{-3} mmHg[55], two orders of magnitude lower than that of phenol (0.35 mmHg[55]) and *p*BQ (0.1 mmHg[55]). In addition, we present the most accurate set of TCSs ever obtained with our experimental setup in terms of energy resolution, reaching around 100 meV at lower collision energies. This was paramount for resolving many of the resonant features in the TCS.

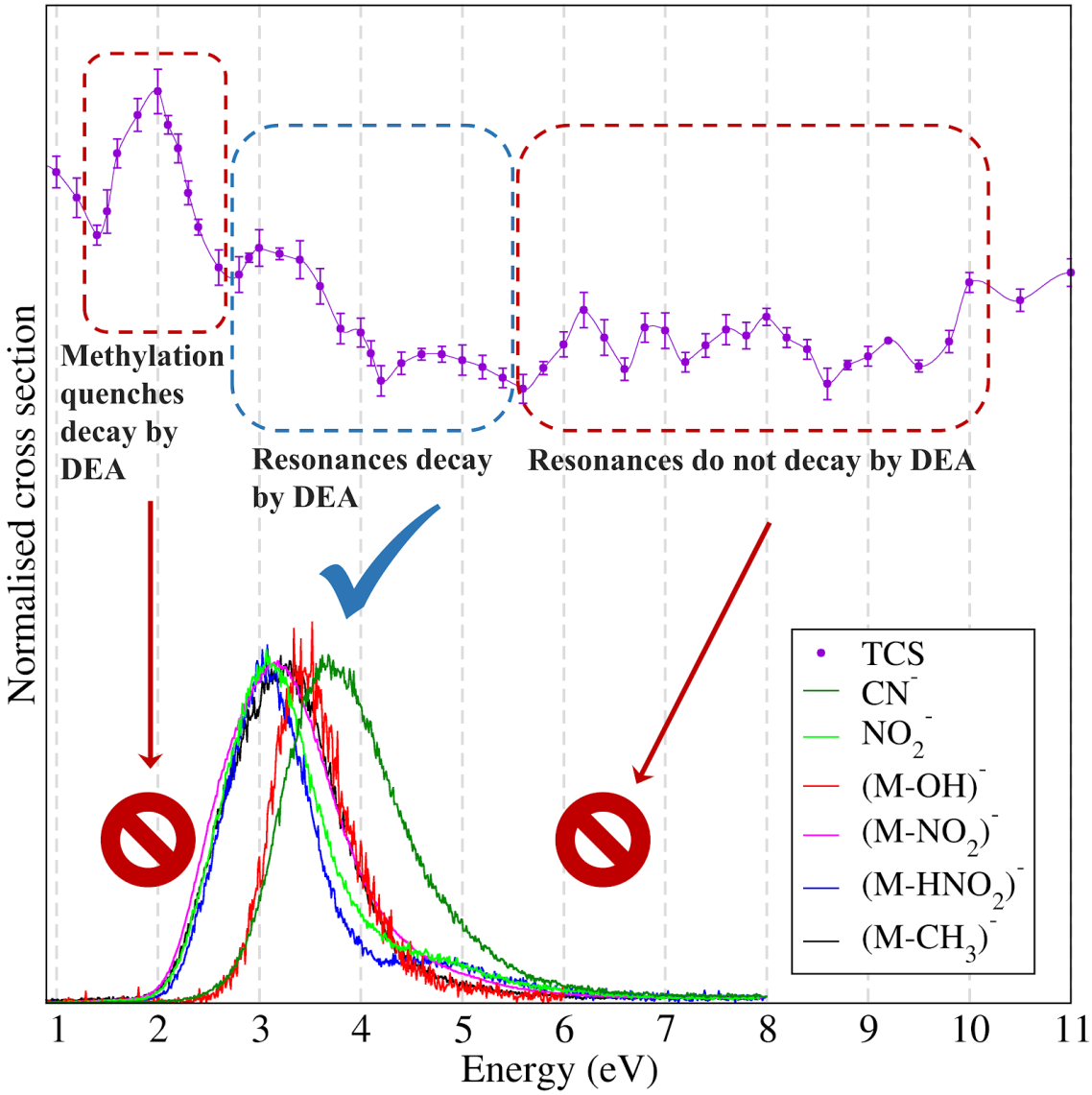

Figure 1. Comparison between our measured TCSs (top) and the ion yields obtained in Ref. 29 (bottom), with maxima normalized to the same value. The line for the TCS is just a guide for the eye.

In Figure 1, we show our measured TCS, revealing a multitude of resonances formed upon electron collisions with 1M5NI. When compared with the ion yields obtained by Tanzer *et al.*[29], we notice that only those resonances located between around 2 and 6 eV decay efficiently by DEA. In contrast, we find several overlapping features at higher energies (see Figure 1 and Table S3), related to core-excited resonances. Surprisingly, none of these higher-lying resonances have been observed in DEA experiments[29]. Therefore, DEA is largely inefficient for the resonances found in the 6 to 10 eV energy range. We thus get to the important conclusion that alternative and efficient decay channels come into play, which may or may not be dissociative. In the former scenario, only neutral fragments should be formed (since there is no signal of DEA).

We argue that neutral dissociation through catalytic electrons[6,7] (shown schematically in Figure 2 in comparison to DEA) should play a big role in the relaxation of these higher-lying resonances. Once the resonance is formed, the electron can be ejected with most of the excess energy, leaving the target molecule in its electronic ground state, but this would be an unlikely two-particle process. Instead, electron detachment

may leave an electronically excited state behind, a more likely one-particle process. There is evidence that the excited states of 1M5NI dissociate into neutral fragments, though not radiatively or via internal conversion to the ground state[37]. Yu *et al.*[37] investigated by experimental and theoretical methods the decomposition of NIs, including 1M5NI, upon photoexcitation in the 5.0 to 5.5 eV range. They found the NO• radical as a product, which would be formed along the potential energy surface of the S_1 excited state, after an internal conversion from the initially excited S_2 state. Our MRCI calculations confirmed the $n_- \pi_1^*$ (S_1) and $n_+ \pi_1^*$ (S_2) character of these states[37] (see results in the Supporting Information). The same dissociation mechanism would be accessible once the S_2 state is populated after electron collisions. The higher-lying resonances we find in the TCS may decay to higher-lying neutral excited states, followed by a series of internal conversions before reaching the S_2 state and dissociating into the NO• radical. On the other hand, entirely different dissociation channels may be accessed from the higher-lying resonances, but again, leading only to uncharged fragments. It is worth mentioning that the NO• radical is itself a radiosensitizer[20]. From the above arguments and the available results on photodissociation of 1M5NI, we believe that dissociation into neutral fragments probably plays an important role in the overall electron-induced chemistry of 1M5NI and NIs in general. Such processes cannot be probed in DEA experiments, limited to detecting charged species. The prevalence of such processes remains largely unknown, but our results suggest that they may be more common than previously thought.

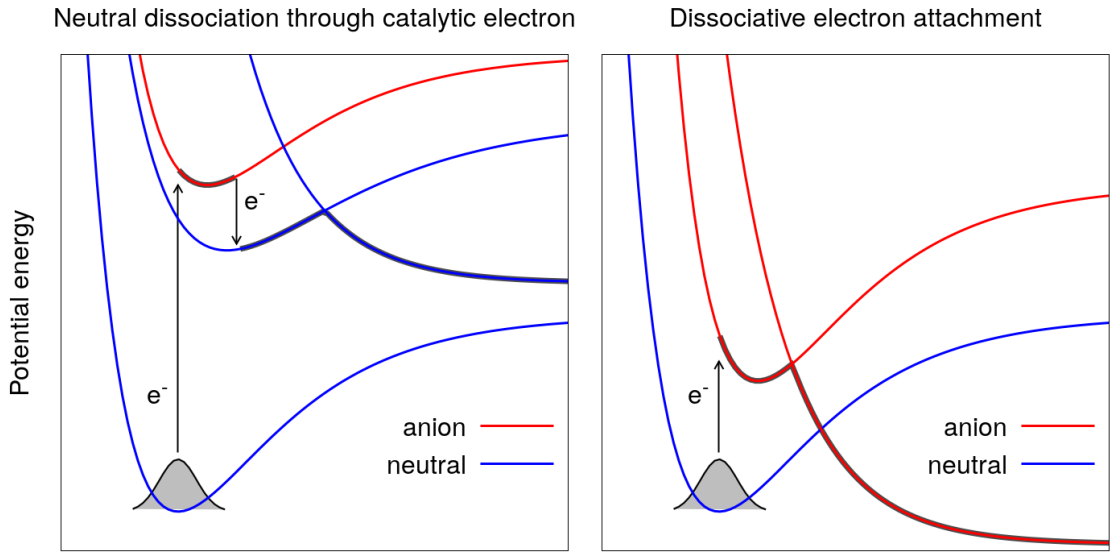

Figure 2. Schematic potential energy curves as function of a reactive coordinate, illustrating two mechanisms for electron-induced chemistry: neutral dissociation through catalytic electron (left) and dissociative electron attachment (right).

The following results and discussion concern the lower energies, where DEA (depicted in Figure 2) is known to occur. The lowest lying structures (below and around 4 eV) were interpreted in light of MRCI/CCSD(T) calculations (see Computational methods and Supporting Information for details). Our results for the three lowest-lying valence anion states are in line with the previous work for these states: there is a bound state (π_1^*), and two shape resonances (π_2^* and π_3^*)[41]. The character of the orbitals relevant for the discussion can be seen in Figure S1. From our experimental TCS and calculations, we have further identified and characterized the four lowest-lying core-excited resonances, all of them involving double occupation of the π_1^* orbital. Table S3

summarizes every structure found in the TCS, as well as our assignments based on the MRCI/CCSD(T) results.

The most prominent peak in our measured TCSs appears between 1.4 and 2.4 eV, peaking at 2.0 eV. This structure is interpreted as the π_2* shape resonance, theoretically characterized in Ref. 41. Our measurements thus provide the first experimental confirmation of the π_2* anion state in 1M5NI. No signature of this state has been observed in DEA experiments to 1M5NI, only in its non-methylated form, implying that methylation quenches DEA reactions below ~2 eV[28,29]. This comparison highlights the ability of our measurements to identify states which may not manifest in other experimental techniques, as also illustrated in Figure 1. Calculations from Kossoski and Varella[41] suggested that the quenching of DEA reactions below 2 eV would be explained by the very short lifetime against autodetachment of the π_2* resonance in 1M5NI. The favorable comparison between the experimental width (0.71 eV, fitting details are given in the Supporting Information) and the calculated one (0.53 eV) lend support to this hypothesis. We recall that fixed-nuclei scattering calculations produce too narrow resonance peaks, such that the purely electronic resonance width from the calculations should be taken as a lower bound to the experiment, making the above difference more reasonable.

The second most prominent feature in our measured TCS is placed between 2.5 eV and 4.2 eV. The experimental maximum (3.2 eV) compares very favorably with the calculated ones for the π_3* shape resonance (3.22 eV with the SMC and 3.12 eV with the MRCI/CCSD(T) calculations). In contrast, the experimental resonance width (1.36 eV) is much larger than the calculated one (0.51 eV). We notice, however, that this peak is considerably more asymmetric than the lower-lying one, with a clear shoulder around 4.0 eV suggesting the presence of other underlying resonances. Indeed, our MRCI/CCSD(T) results support four core-excited resonances between 3.5 and 4.3 eV (see Table S2). From the favorable theoretical-experimental comparisons regarding the π_2* and π_3* shape resonances, we believe that the core-excited resonances would be similarly well described in our calculations, with errors probably below 0.3 eV. We therefore assign the 4.0 eV shoulder to the π_O $(\pi_1^*)^2$ core-excited resonance, theoretically predicted at 3.97 eV. Meanwhile, the 3.2 eV peak should stem from the π_3* shape resonance, with some minor contribution from the n_- $(\pi_1^*)^2$ core-excited resonance, theoretically found at 3.12 eV and 3.55 eV, respectively.

Further insights about the underlying DEA reactions are gained once we compare our results with the ion yields reported by Tanzer *et al.*[29], shown in Figure 1. Above 2 eV, we identify three distinct energy ranges in their measured ion yields. The first one extends from 2 to 6 eV, peaking at around 3 eV, and is common to all fragments involving the nitro group and loss of the methyl group. These DEA channels would be triggered by the π_3* anion state (in the present work at ~3.2 eV), which couples to dissociative anion states along the C-NO_2 or N-CH_3 bond[41]. We notice the competition among several dissociation channels for the same resonance. In contrast, production of $(1M5NI\text{-}OH)^-$ has a distinct profile, narrower in energy and peaking at ~3.4 eV. We assign this fragment to the formation of the n_- $(\pi_1^*)^2$ core-excited resonance (found at 3.55 eV in the present calculations). In turn, the CN^- yield has a maximum at ~3.8 eV, and shows a broader energy profile. This DEA channel may be triggered by the π_O $(\pi_1^*)^2$ core-excited resonance (identified here at 3.97 eV). Note that the above assignments concern the resonance that probably has the largest contribution to each dissociation channel. In fact, the fairly broad energy profiles in the ion yields suggest that all these resonances probably contribute to the same DEA channels. Ribar *et al.*[30] already suggested the existence of a

π $(\pi^*)^2$ core-excited resonance at ~3.5 eV, based on the prior observations of a shake-up satellite in X-ray photoelectron spectra of NIs[40] and also on electron transmission studies on nitroaromatic compounds[56]. Our results support the presence of such a core-excited resonance, and further provide its specific character as π_O $(\pi_1^*)^2$. This resonance involves mostly the nitro group, despite some conjugation of the π_1^* orbital with the imidazole group (see Figure S1). As such, it should be common for nitro-containing compounds. Besides the immediate connection to the above-mentioned studies[40,56], we further relate the 4 eV shoulder in the TCS (Figure 1) to the peak recently observed in the nitrobenzene TCS measurements at around the same energy[57].

Extending from 4.2 to 5.6 eV, there is a broad and somewhat asymmetric feature, with a maximum at ~4.7 eV, and likely originating from the contribution of several core-excited resonances. Tanzer *et al*.[29] mentioned that structures in the high-energy tail of their measured ion yields could be related to the opening of dissociation channels into more than one neutral species. While this can be an important aspect to consider, the observation of such structures in their ion yields means that additional underlying resonances trigger the dissociation. Indeed, the weak shoulders observed in DEA experiments would be related to some of the higher-lying resonances found in our TCS measurements. The higher-lying roots of our MRCI/CCSD(T) calculations (Table S2) are contained in this region: a π_1 $(\pi_1^*)^2$ core-excited resonance at 4.23 eV and a n_+ $(\pi_1^*)^2$ core-excited resonance at 4.26 eV, though probably more resonances contribute to this broad structure. The only signals in DEA experiments which can be directly correlated with the TCS feature are the formation of NO_2^- and $(1M5NI\text{-}HNO_2)^-$. As discussed above, smaller contributions from higher-lying resonances are expected for most fragments, in view of their generally broad energy profiles. However, it is surprising that resonances displaying a clear rise in the TCS have such a small contribution to DEA (see Figure 1). Except for the somewhat larger signals of $(4(5)NI\text{-}HNO_2)^-$ in this energy range, the ion yields for the non-methylated compound are quite similar[28,29], meaning that a quenching mechanism due to methylation cannot be implied here.

Our TCS further reveals a resonance centered at 6.2 eV, extending from 5.6 to 6.6 eV. It has no obvious correspondence to the ion yield measurements for 1M5NI (neither for 1M4NI)[29], showing that the underlying resonances do not lead to DEA reactions. In this case, however, 4(5)NI actually undergoes DEA at around the same energies, with distinct features observed for several fragments[29]. Based on the rather similar energies for the lower-lying resonances[29,41], the same would be expected for the resonance(s) at ~6 eV. We deduce from the observation of the figures in Ref. 29 that methylation not only quenches DEA reactions below 2 eV[28,29], but also around 6 eV. Even then, it is remarkable that the 6.2 eV peak in our TCS is rather intense when compared with the lower-lying structures, whereas in DEA experiments the signals around 6.2 eV are much weaker than in lower energies. This suggests that these resonances also decay more efficiently by other mechanisms, as discussed above for the higher-lying resonances.

The measured TCS also served to assess the performance of two *ab-initio* electron scattering methodologies, the SMC method for the lower energies, and the IAM-SCAR+I method for the intermediate and higher energies, as shown in Figure 3. To properly compare experimental and theoretical cross sections, special precautions are needed. For each impact energy, we integrated the calculated DCSs over the experimental angular acceptance range, thus ignoring the contribution from forward and backward "missing angles" (MA) (see experimental methods for details). Then, the integrated cross sections were convoluted with a Gaussian having the width of the experimental energy resolution. The final results are depicted in Figure 3 as SMC-MA (elastic) and IAM-SCAR+I-MA

(elastic). Adding the inelastic cross sections (ionization and electronic excitation) to the latter further provides a TCS that can be directly compared with the experimental data.

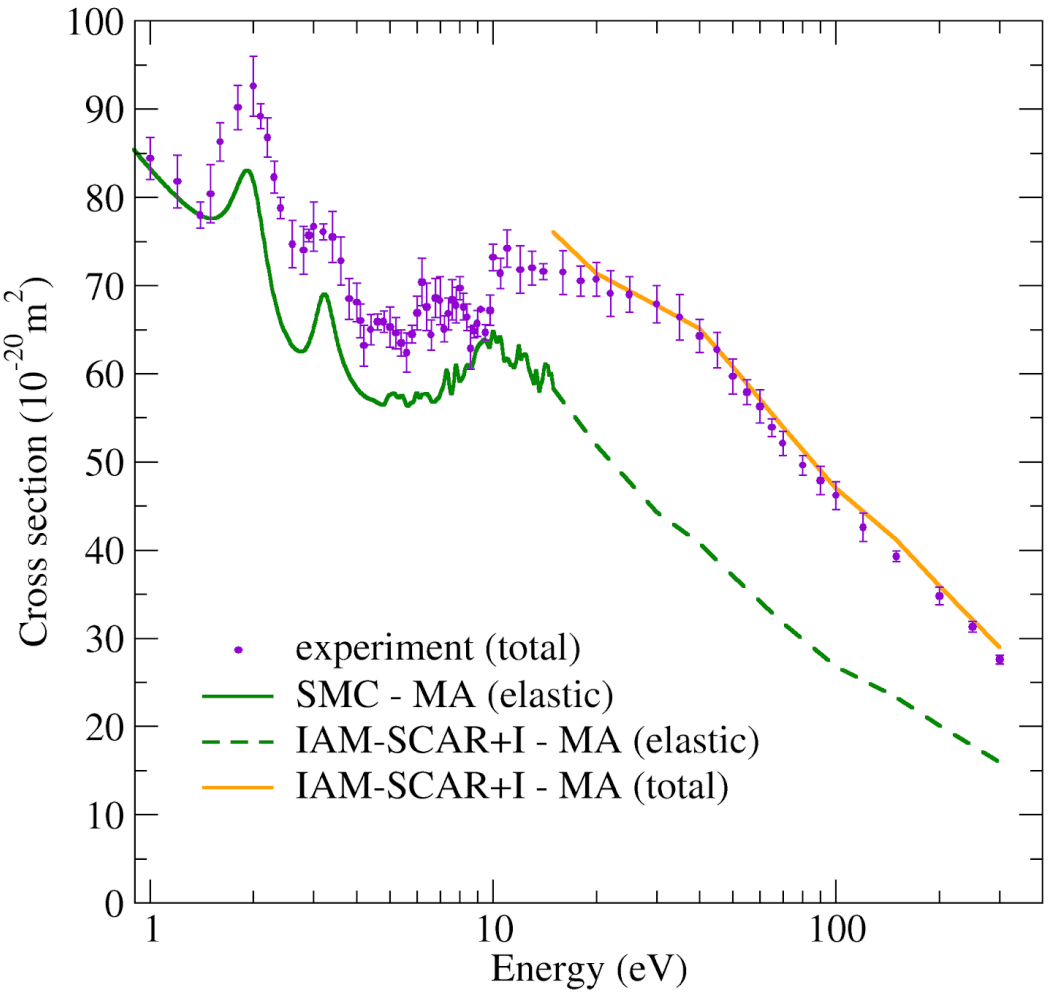

Figure 3. Experimental total electron scattering cross sections from 1M5NI in the energy range 1-300 eV, together with our IAM-SCAR+I and (elastic) SMC results, considering the experimental angular acceptance (see text for further details).

Both magnitudes and the overall shape of TCSs compare quite favorably, which is reassuring for both experimental and theoretical methodologies. The elastic cross sections computed with the SMC method clearly indicate the dominance of the elastic channel at lower energies. The theoretical magnitudes appear somewhat underestimated though, which remains to be understood. The positions of the two lowest lying resonances (around 2.0 eV and 3.2 eV) are correctly reproduced. The same can be said about the rise of the cross sections at lower energies, related to the long-range interaction mediated by the permanent dipole moment of 1M5NI (4.37 D[58]). Above 4 eV, several weaker features appear in the computed cross sections, which should not be interpreted as physical, given the lack of open electronic excitation channels in our model. The level of agreement between the experiment and the IAM-SCAR+I calculations is excellent at higher energies, but no longer holds below ~15eV (not shown), where the IAM-SCAR+I method cannot provide reliable cross sections[54,59,60]. Even so, it is worth mentioning the good

matching at around 15 eV between the SMC and the (elastic) IAM-SCAR+I results. Finally, the TCS for 1M5NI lies around 10^{-18} m^2 at the lower energies (~1 eV), which is of the same order of magnitude as the associative electron attachment cross sections reported for metronidazole ($3.6x10^{-18}$ m^2)[33] and nimorazole ($2.8x10^{-18}$ m^2)[31] close to 0 eV. Despite the different impact energies, systems, and processes, this comparison helps to put the latter cross sections in perspective, highlighting the relevance of associative attachment for metronidazole and nimorazole.

To summarize, here we have employed a state-of-the-art experimental setup for measuring total electron scattering cross sections from 1M5NI, a model molecule for the important class of nitroimidazolic radiosensitizers. The high accuracy and energy resolution reached in the present experiment has allowed us to accurately identify many resonances in the TCS, associated with the formation of transient anions. Our main finding is that several of these resonances have no parallel in DEA experiments, showing that alternative decay mechanisms are operative. These higher-lying states are expected to eject slow electrons, thereby populating neutral excited states, which are known to dissociate into neutral fragments based on photodissociation studies from Yu *et al.*[36]. We conclude that such neutral dissociation through catalytic electrons mechanism should play a big role in the electron induced decomposition of 1M5NI. Importantly, this mechanism would be accessible for a rather wide energy range (6 to 10 eV, see Figure 1), where no DEA takes place. This is an important energy range in the context of radiosensitivity because it coincides with the maximum of the energy distribution of the secondary electrons produced inside biological matter[23]. Having only this aspect in mind, processes occurring in the above energy range (like the neutral dissociation we propose) would be more frequent than those at lower energies (such as DEA), at least in the early stages of thermalization. We notice, however, that the secondary electrons quickly lose their energy to the medium and form much lower energy pre-solvated states[15], which could still lead to DEA reactions. Furthermore, neutral dissociation events are expected to be even more chemically relevant than DEA events breaking a single bond, because two radical species (and a released electron) are produced in the former, against only one radical in the latter. While DEA is believed to be a major contributor to understanding radiosensitivity[12-16], our results point out neutral dissociation through catalytic electrons as a new pathway for radiosensitization. In particular, this pathway represents an alternative radiosensitizing mechanism for nitroimidazolic radiosensitizers, which could play a similarly important role as the previously proposed associative attachment (for nimorazole[31] and metronidazole[33]) and DEA (for smaller NIs[28-30]) electron-induced processes. Detection of neutral fragments remains one of the main experimental challenges in the field of electron-molecule interactions, and we expect our contribution will further encourage the community into looking at this missing puzzle[61,62]. Our results also shed new light on the transient anions and dissociation pathways of 1M5NI below 4 eV, and on the effect of methylation in suppressing DEA reactions between 4 and 6 eV. Finally, the present study demonstrates that accurate measurements of absolute TCS for solid compounds having a room temperature vapor pressure as low as ~10^{-3} mmHg are technically feasible. This opens the possibility of performing analogous studies for electron interactions with molecules having comparable low vapor pressures.

Experimental methods

The TCSs measurements have been carried out in a state-of-the-art magnetically confined electron beam system described in detail elsewhere[60,63]. Further details about the experimental methods can be found in Section S1 of the Supporting Information. Considering that 1M5NI is solid and has a very low vapor pressure at room temperature

(~1.7×10^{-3} mmHg[55]), obtaining the present measurements has represented a major experimental challenge. The main reason is that absolute values of TCS require accurate and stable measurements of the sample's gas pressure inside the collision chamber, which becomes increasingly more difficult for compounds of lower vapor pressures. The sample was heated up to around 333 K. At the same time, the temperature was controlled to maintain it in a range where thermal dissociation does not occur. In addition, the collision chamber's temperature was kept at around 20 to 30 K above the sample's temperature, thus preventing condensation effects.

Although the total statistical uncertainties of the present measurements remain below 5%, our measured TCSs lay lower than the "real" values due to the experimental angular acceptance. Concretely, in the present experimental system, the angular resolution is linked to the energy resolution as a consequence of the magnetic confinement, entailing thus "missing angles" in the forward and backward scattering directions, as explained in detail in Ref. 63. Therefore, this should be considered when the results derived from this setup are compared with other, experimental[60,64] but also theoretical results. The present experimental TCSs together with their absolute uncertainties are available in Table S1.

Computational methods

To quantitatively characterize the lower-lying shape and core-excited resonances of 1M5NI, we resorted to bound-state MRCI calculations. By building proper state-average reference wave functions, we aim at a more balanced description of both (one-particle) shape and (two-particle) core-excited resonances. Being a bound-state method, couplings to the continuum are neglected. However, we verified that all the obtained roots correspond to localized states (and not some discretization of the continuum), thus reassuring that our MRCI calculations would provide a decent description of the resonances. The relative energies among neutral states and among anion states are expected to be reasonable with our MRCI calculations. That would not be the case, however, when comparing neutral and anion energies, since the latter appear too high with respect to the former. This is due to the well-known challenges associated with a balanced description of correlation effects in neutral and charged forms. In order to correct for that, we have performed separate calculations for the neutral and anion ground states, at the coupled cluster with singles, doubles, and perturbative triples [CCSD(T)] level[65,66]. Then, we introduced a systematic shift to all energies of the anion states, based on the CCSD(T) binding energy. More precisely, the herein reported resonance energy for the i-th anion state, E_r^i, was obtained as $E^i{}_r = E^1{}_{CCSD(T)} - E^N{}_{CCSD(T)} + E^i{}_{MRCI} - E^N{}_{MRCI}$, where $E^1{}_{CCSD(T)}$ and $E^N{}_{CCSD(T)}$ are the CCSD(T) energies of the anion ground state (i=1) and of the neutral ground state, and $E^i{}_{MRCI}$ and $E^N{}_{MRCI}$ are the MRCI energies (plus Pople's extensivity correction[67]) of the i-th anion state and of the neutral ground state. Throughout the text, we refer to this mixed set of calculations as MRCI/CCSD(T). Due to the high computational cost of these calculations, a limited number of states was obtained (seven for each charge state), thus restricting our theoretical analysis to energies below ~4 eV.

Further methodological details concerning the bound-state MRCI and electron scattering IAM-SCAR+I and SMC calculations are given in Section S2 of the Supporting Information. We notice that the current implementation of the SMC method usually provides one-particle shape resonance energies to within ~0.3 eV of the experimental values, though it still struggles to describe two-particle core-excited resonances[68,69]. For this reason, we resorted to bound-state MRCI calculations to describe these states.

Acknowledgements

This study has been partially supported by the Spanish Ministerio de Ciencia e Innovación (Project PID2019-104727RB-C21), Ministerio de Universidades (Project PRX21/00340) and CSIC (Project LINKA20085). AIL and PL-V acknowledge the Portuguese National Funding Agency (FCT) through research Grants CEFITEC (UIDB/00068/2020) and PTDC/FIS-AQM/31281/2017. MTNV acknowledges the Brazilian National Council for Scientific and Technological Development (CNPq), grant No. 304571/2018-0, and the São Paulo Research Foundation (FAPESP), grant No. 2020/16155-7. We also thank Prof. Stephan Denifl from the University of Innsbruck for providing published data on DEA to 1M5NI.

Supporting Information Available

Experimental and theoretical details, measured total electron scattering cross sections and their absolute uncertainties, active orbitals in the CASSCF calculations, vertical excitation energies, resonance energies of the anion states, and Gaussian fit of the two lowest-lying peaks.

References

(1) Schulz, G. J. Resonances in Electron Impact on Diatomic Molecules. *Rev. Mod. Phys.* **1973**, *45* (3), 423–486.

(2) Fabrikant, I. I.; Eden, S.; Mason, N. J.; Fedor, J. Recent Progress in Dissociative Electron Attachment. In *Advances in Atomic, Molecular, and Optical Physics*; 2017; pp 545–657.

(3) Ingolfsson, O. *Low-Energy Electrons: Fundamentals and Applications*; Jenny Stanford Publishing: Boca Raton, 2019.

(4) Pshenichnyuk, S. A.; Modelli, A.; Komolov, A. S. Interconnections between Dissociative Electron Attachment and Electron-Driven Biological Processes. *Int. Rev. Phys. Chem.* **2018**, *37* (1), 125–170.

(5) Pshenichnyuk, S. A.; Asfandiarov, N. L.; Vorob'ev, A. S.; Matejčík, Š. State of the Art in Dissociative Electron Attachment Spectroscopy and Its Prospects. *Physics-Uspekhi* **2022**, *65* (2), 163–188.

(6) Davis, D.; Vysotskiy, V. P.; Sajeev, Y.; Cederbaum, L. S. Electron Impact Catalytic Dissociation: Two-Bond Breaking by a Low-Energy Catalytic Electron. *Angew. Chemie Int. Ed.* **2011**, *50* (18), 4119–4122.

(7) Davis, D.; Vysotskiy, V. P.; Sajeev, Y.; Cederbaum, L. S. A One-Step Four-Bond-Breaking Reaction Catalyzed by an Electron. *Angew. Chemie Int. Ed.* **2012**, *51* (32), 8003–8007.

(8) Davis, D.; Kundu, S.; Prabhudesai, V. S.; Sajeev, Y.; Krishnakumar, E. Formation of CO_2 from Formic Acid through Catalytic Electron Channel. *J. Chem. Phys.* **2018**, *149* (6), 064308.

(9) Brunger, M. J. Molecular Processes and Techniques for Measuring Their Scattering Cross Sections. In *Low-Energy Electrons*; Jenny Stanford Publishing, 2019; pp 1–46.

(10) Szmytkowski, C.; Możejko, P. Recent Total Cross Section Measurements in Electron Scattering from Molecules. *Eur. Phys. J. D* **2020**, *74* (5), 90.

(11) Jordan, K. D.; Burrow, P. D. Temporary Anion States of Polyatomic Hydrocarbons. *Chem. Rev.* **1987**, *87* (3), 557–588.

(12) Alizadeh, E.; Orlando, T. M.; Sanche, L. Biomolecular Damage Induced by Ionizing Radiation: The Direct and Indirect Effects of Low-Energy Electrons on DNA. *Annu. Rev. Phys. Chem.* **2015**, *66* (1), 379–398.

(13) Schürmann, R.; Tsering, T.; Tanzer, K.; Denifl, S.; Kumar, S. V. K.; Bald, I. Resonant Formation of Strand Breaks in Sensitized Oligonucleotides Induced by Low-Energy Electrons (0.5-9 eV). *Angew. Chemie Int. Ed.* **2017**, *56* (36), 10952–10955.

(14) Schürmann, R.; Vogel, S.; Ebel, K.; Bald, I. The Physico-Chemical Basis of DNA Radiosensitization: Implications for Cancer Radiation Therapy. *Chem. - A Eur. J.* **2018**, *24* (41), 10271–10279.

(15) Kumar, A.; Becker, D.; Adhikary, A.; Sevilla, M. D. Reaction of Electrons with DNA: Radiation Damage to Radiosensitization. *Int. J. Mol. Sci.* **2019**, *20* (16), 3998.

(16) Ebel, K.; Bald, I. Low-Energy (5–20 eV) Electron-Induced Single and Double Strand Breaks in Well-Defined DNA Sequences. *J. Phys. Chem. Lett.* **2022**, 4871–4876.

(17) Arumainayagam, C. R.; Lee, H.-L.; Nelson, R. B.; Haines, D. R.; Gunawardane, R. P. Low-Energy Electron-Induced Reactions in Condensed Matter. *Surf. Sci. Rep.* **2010**, *65* (1), 1–44.

(18) Böhler, E.; Warneke, J.; Swiderek, P. Control of Chemical Reactions and Synthesis by Low-Energy Electrons. *Chem. Soc. Rev.* **2013**, *42* (24), 9219–9231.

(19) Arumainayagam, C. R.; Garrod, R. T.; Boyer, M. C.; Hay, A. K.; Bao, S. T.; Campbell, J. S.; Wang, J.; Nowak, C. M.; Arumainayagam, M. R.; Hodge, P. J. Extraterrestrial Prebiotic Molecules: Photochemistry vs. Radiation Chemistry of Interstellar Ices. *Chem. Soc. Rev.* **2019**, *48* (8), 2293–2314.

(20) Wardman, P. Chemical Radiosensitizers for Use in Radiotherapy. *Clin. Oncol.* **2007**, *19* (6), 397–417.

(21) Gong, L.; Zhang, Y.; Liu, C.; Zhang, M.; Han, S. Application of Radiosensitizers in Cancer Radiotherapy. *Int. J. Nanomedicine* **2021**, *Volume 16*, 1083–1102.

(22) Zdrowowicz, M.; Chomicz-Mańka, L.; Butowska, K.; Spisz, P.; Falkiewicz, K.; Czaja, A.; Rak, J. DNA Damage Radiosensitizers Geared Towards Hydrated Electrons. In *Practical Aspects of Computational Chemistry V*; Springer International Publishing: Cham, 2022; pp 125–169.

(23) Pimblott, S. M.; LaVerne, J. A. Production of Low-Energy Electrons by Ionizing Radiation. *Radiat. Phys. Chem.* **2007**, *76* (8–9), 1244–1247.

(24) Alizadeh, E.; Sanche, L. Precursors of Solvated Electrons in Radiobiological Physics and Chemistry. *Chem. Rev.* **2012**, *112* (11), 5578–5602.

(25) Gorfinkiel, J. D.; Ptasinska, S. Electron Scattering from Molecules and Molecular Aggregates of Biological Relevance. *J. Phys. B At. Mol. Opt. Phys.* **2017**, *50* (18), 182001.

(26) Wang, H.; Mu, X.; He, H.; Zhang, X.-D. Cancer Radiosensitizers. *Trends Pharmacol. Sci.* **2018**, *39* (1), 24–48.

(27) Henk, J. M.; Bishop, K.; Shepherd, S. F. Treatment of Head and Neck Cancer with CHART and Nimorazole: Phase II Study. *Radiother. Oncol.* **2003**, *66* (1), 65–70.

(28) Tanzer, K.; Feketeová, L.; Puschnigg, B.; Scheier, P.; Illenberger, E.; Denifl, S. Reactions in Nitroimidazole Triggered by Low-Energy (0 - 2 eV) Electrons: Methylation at N1-H Completely Blocks Reactivity. *Angew. Chemie - Int. Ed.* **2014**, *53* (45), 12240–12243.

(29) Tanzer, K.; Feketeová, L.; Puschnigg, B.; Scheier, P.; Illenberger, E.; Denifl, S. Reactions in Nitroimidazole and Methylnitroimidazole Triggered by Low-Energy (0-8 eV) Electrons. *J. Phys. Chem. A* **2015**, *119* (25), 6668–6675.

(30) Ribar, A.; Fink, K.; Probst, M.; Huber, S. E.; Feketeová, L.; Denifl, S. Isomer Selectivity in Low-Energy Electron Attachment to Nitroimidazoles. *Chem. - A Eur. J.* **2017**, *23* (52), 12892–12899.

(31) Meißner, R.; Kočišek, J.; Feketeová, L.; Fedor, J.; Fárník, M.; Limão-Vieira, P.; Illenberger, E.; Denifl, S. Low-Energy Electrons Transform the Nimorazole Molecule into a Radiosensitiser. *Nat. Commun.* **2019**, *10* (1), 2388.

(32) Meißner, R.; Feketeová, L.; Illenberger, E.; Denifl, S. Reactions in the Radiosensitizer Misonidazole Induced by Low-Energy (0–10 eV) Electrons. *Int. J. Mol. Sci.* **2019**, *20* (14), 3496.

(33) Lochmann, C.; Luxford, T. F. M.; Makurat, S.; Pysanenko, A.; Kočišek, J.; Rak, J.; Denifl, S. Low-Energy Electron Induced Reactions in Metronidazole at Different Solvation Conditions. *Pharmaceuticals* **2022**, *15* (6), 701.

(34) Cho, J. R.; Kim, K. J.; Cho, S. G.; Kim, J. K. Synthesis and Characterization of 1-Methyl-2,4,5-Trinitroimidazole (MTNI). *J. Heterocycl. Chem.* **2002**, *39* (1), 141–147.

(35) Nair, U.; Asthana, S.; Rao, A.; Gandhe, B. Advances in High Energy Materials. *Def. Sci. J.* **2010**, *60* (2), 137–151.

(36) Yu, Z.; Bernstein, E. R. Experimental and Theoretical Studies of the Decomposition of New Imidazole Based Energetic Materials: Model Systems. *J. Chem. Phys.* **2012**, *137* (11), 114303.

(37) Yu, Z.; Bernstein, E. R. On the Decomposition Mechanisms of New Imidazole-Based Energetic Materials. *J. Phys. Chem. A* **2013**, *117* (8), 1756–1764.

(38) Carvalho, T. M. T.; Amaral, L. M. P. F.; Morais, V. M. F.; Ribeiro da Silva, M. D. M. C. Calorimetric and Computational Studies for Three Nitroimidazole Isomers. *J. Chem. Thermodyn.* **2017**, *105*, 267–275.

(39) Feketeová, L.; Plekan, O.; Goonewardane, M.; Ahmed, M.; Albright, A. L.; White, J.; OHair, R. A. J.; Horsman, M. R.; Wang, F.; Prince, K. C. Photoelectron Spectra and Electronic Structures of the Radiosensitizer Nimorazole and Related Compounds. *J. Phys. Chem. A* **2015**, *119* (39), 9986–9995.

(40) Itälä, E.; Tanzer, K.; Granroth, S.; Kooser, K.; Denifl, S.; Kukk, E. Fragmentation Patterns of 4(5)-Nitroimidazole and 1-Methyl-5-Nitroimidazole — The Effect of the Methylation. *J. Mass Spectrom.* **2017**, *52* (11), 770–776.

(41) Kossoski, F.; Varella, M. T. do N. How Does Methylation Suppress the Electron-Induced Decomposition of 1-Methyl-Nitroimidazoles? *J. Chem. Phys.* **2017**, *147* (16), 164310.

(42) Mendes, M.; Probst, M.; Maihom, T.; García, G.; Limão-Vieira, P. Selective Bond Excision in Nitroimidazoles by Electron Transfer Experiments. *J. Phys. Chem. A* **2019**, *123* (18), 4068–4073.

(43) Mendes, M.; García, G.; Bacchus-Montabonel, M. C.; Limão-Vieira, P. Electron Transfer Induced Decomposition in Potassium–Nitroimidazoles Collisions: An Experimental and Theoretical Work. *Int. J. Mol. Sci.* **2019**, *20* (24), 1–18.

(44) Szalay, P. G.; Müller, T.; Gidofalvi, G.; Lischka, H.; Shepard, R. Multiconfiguration Self-Consistent Field and Multireference Configuration Interaction Methods and Applications. *Chem. Rev.* **2012**, *112* (1), 108–181.

(45) Takatsuka, K.; McKoy, V. Extension of the Schwinger Variational Principle beyond the Static-Exchange Approximation. *Phys. Rev. A* **1981**, *24* (5), 2473–2480.

(46) da Costa, R. F.; Varella, M. T. do N.; Bettega, M. H. F.; Lima, M. A. P. Recent Advances in the Application of the Schwinger Multichannel Method with

Pseudopotentials to Electron-Molecule Collisions. *Eur. Phys. J. D* **2015**, *69* (6), 159.

(47) Blanco, F.; García, G. Screening Corrections for Calculation of Electron Scattering Differential Cross Sections from Polyatomic Molecules. *Phys. Lett. A* **2004**, *330* (3–4), 230–237.

(48) Blanco, F.; Rosado, J.; Illana, A.; García, G. Comparison of Two Screening Corrections to the Additivity Rule for the Calculation of Electron Scattering from Polyatomic Molecules. *Phys. Lett. A* **2010**, *374* (43), 4420–4424.

(49) Blanco, F.; Ellis-Gibbings, L.; García, G. Screening Corrections for the Interference Contributions to the Electron and Positron Scattering Cross Sections from Polyatomic Molecules. *Chem. Phys. Lett.* **2016**, *645*, 71–75.

(50) Dubuis, A. T.; Costa, F.; da Silva, F. F.; Limão-Vieira, P.; Oller, J. C.; Blanco, F.; García, G. Total Electron Scattering Cross Section from Pyridine Molecules in the Energy Range 10–1000 eV. *Chem. Phys. Lett.* **2018**, *699*, 182–187.

(51) Chernyshova, I. V.; Kontrosh, E. E.; Markush, P. P.; Shpenik, O. B. The Interaction of Low-Energy Electrons with Fructose Molecules. *Tech. Phys. Lett.* **2017**, *43* (11), 998–1000.

(52) Chernyshova, I. V.; Kontrosh, E. E.; Shpenik, O. B. Collisions of Slow Electrons with Thymine Molecules. *Opt. Spectrosc.* **2018**, *125* (6), 845–852.

(53) da Costa, R. F.; de Oliveira, E. M.; Bettega, M. H. F.; Varella, M. T. do N.; Jones, D. B.; Brunger, M. J.; Blanco, F.; Colmenares, R.; Limão-Vieira, P.; García, G.; Lima, M. A. P. Electron Collisions with Phenol: Total, Integral, Differential, and Momentum Transfer Cross Sections and the Role of Multichannel Coupling Effects on the Elastic Channel. *J. Chem. Phys.* **2015**, *142* (10), 104304.

(54) Lozano, A. I.; Oller, J. C.; Jones, D. B.; da Costa, R. F.; Varella, M. T. do N.; Bettega, M. H. F.; Ferreira da Silva, F.; Limão-Vieira, P.; Lima, M. A. P.; White, R. D.; Brunger, M. J.; Blanco, F.; Muñoz, A.; García, G. Total Electron Scattering Cross Sections from Para-Benzoquinone in the Energy Range 1–200 eV. *Phys. Chem. Chem. Phys.* **2018**, *20* (34), 22368–22378.

(55) U.S. National Library of Medicine. https://chem.nlm.nih.gov (accessed 2022-06-01).

(56) Modelli, A.; Venuti, M. Empty Level Structure and Dissociative Electron Attachment in Gas-Phase Nitro Derivatives. *Int. J. Mass Spectrom.* **2001**, *205* (1–3), 7–16.

(57) Álvarez, L.; Costa, F.; Lozano, A. I.; Oller, J. C.; Muñoz, A.; Blanco, F.; Limão-Vieira, P.; White, R. D.; Brunger, M. J.; García, G. Electron Scattering Cross Sections from Nitrobenzene in the Energy Range 0.4–1000 eV: The Role of Dipole Interactions in Measurements and Calculations. *Phys. Chem. Chem. Phys.* **2020**, *22* (24), 13505–13515.

(58) Pandeti, S.; Feketeová, L.; Reddy, T. J.; Abdoul-Carime, H.; Farizon, B.; Farizon, M.; Märk, T. D. Nitroimidazolic Radiosensitizers Investigated by Electrospray Ionization Time-of-Flight Mass Spectrometry and Density Functional Theory. *RSC Adv.* **2017**, *7* (71), 45211–45221.

(59) Lozano, A. I.; Loupas, A.; Blanco, F.; Gorfinkiel, J. D.; García, G. Total Electron Scattering Cross Sections from Thiophene for the (1-300 eV) Impact Energy Range. *J. Chem. Phys.* **2018**, *149* (13), 134303.

(60) García-Abenza, A.; Lozano, A. I.; Álvarez, L.; Oller, J. C.; Blanco, F.; Stokes, P.; White, R. D.; Urquijo, J. de; Limão-Vieira, P.; Jones, D. B.; Brunger, M. J.; García, G. A Complete Data Set for the Simulation of Electron Transport through Gaseous Tetrahydrofuran in the Energy Range 1–100 eV. *Eur. Phys. J. D* **2021**, *75* (12), 303.

(61) Li, Z.; Milosavljević, A. R.; Carmichael, I.; Ptasinska, S. Characterization of Neutral Radicals from a Dissociative Electron Attachment Process. *Phys. Rev. Lett.* **2017**, *119* (5), 053402.

(62) Ptasinska, S. A Missing Puzzle in Dissociative Electron Attachment to Biomolecules: The Detection of Radicals. *Atoms* **2021**, *9* (4), 77.

(63) Lozano, A. I.; Oller, J. C.; Krupa, K.; Ferreira da Silva, F.; Limão-Vieira, P.; Blanco, F.; Muñoz, A.; Colmenares, R.; García, G. Magnetically Confined Electron Beam System for High Resolution Electron Transmission-Beam Experiments. *Rev. Sci. Instrum.* **2018**, *89* (6), 063105.

(64) Costa, F.; Traoré-Dubuis, A.; Álvarez, L.; Lozano, A. I.; Ren, X.; Dorn, A.; Limão-Vieira, P.; Blanco, F.; Oller, J. C.; Muñoz, A.; García-Abenza, A.; Gorfinkiel, J. D.; Barbosa, A. S.; Bettega, M. H. F.; Stokes, P.; White, R. D.; Jones, D. B.; Brunger, M. J.; García, G. A Complete Cross Section Data Set for Electron Scattering by Pyridine: Modelling Electron Transport in the Energy Range 0–100 eV. *Int. J. Mol. Sci.* **2020**, *21* (18), 6947.

(65) Purvis, G. D.; Bartlett, R. J. A Full Coupled-cluster Singles and Doubles Model: The Inclusion of Disconnected Triples. *J. Chem. Phys.* **1982**, *76* (4), 1910–1918.

(66) Raghavachari, K.; Trucks, G. W.; Pople, J. A.; Head-Gordon, M. A Fifth-Order Perturbation Comparison of Electron Correlation Theories. *Chem. Phys. Lett.* **1989**, *157* (6), 479–483.

(67) Pople, J. A.; Seeger, R.; Krishnan, R. Variational Configuration Interaction Methods and Comparison with Perturbation Theory. *Int. J. Quantum Chem.* **1977**, *12* (S11), 149–163.

(68) da Costa, R. F.; Ruivo, J. C.; Kossoski, F.; Varella, M. T. do N.; Bettega, M. H. F.; Jones, D. B.; Brunger, M. J.; Lima, M. A. P. An Ab Initio Investigation for Elastic and Electronically Inelastic Electron Scattering from Para-Benzoquinone. *J. Chem. Phys.* **2018**, *149* (17), 174308.

(69) Moreira, G. M.; Kossoski, F.; Bettega, M. H. F.; Costa, R. F. da. Electronic Excitation of the $^3B_2$ State of Thiophene Molecule by Low-Energy Electron Collisions. *J. Phys. B At. Mol. Opt. Phys.* **2020**, *53* (8), 085002.